Chemistry Europe

AWARD

Nominate a Worthy Chemist Chemistry Europe Award

Subject:
chemistry for sustainability, energy, materials, environment

Consists of:
prize money amounting to EUR 10,000, certificate

Deadline:
November 1, 2022

▶ **Click here for more info & nomination**

ChemistrySelect

Research Article
doi.org/10.1002/slct.202202287

Check for updates

Chemistry Europe
European Chemical
Societies Publishing

www.chemistryselect.org

Synthesis and X-ray Characterization of 4,5-Dihydropyrazolyl-Thiazoles Bearing a Coumarin Moiety: On the Importance of Antiparallel π-Stacking

Murtaza Madni,[a] Muhammad Naeem Ahmed,*[b] Ghazala Abbasi,[b] Shahid Hameed,*[a] Mahmoud A. A. Ibrahim,[c] Muhammad N.Tahir,[d] Muhammad Ashfaq,[d] Diego M. Gil,[e] Rosa M. Gomila,[f] and Antonio Frontera*[f]

The synthetic protocol and solid state characterization of two new coumarin-pyrazolylthiazole hybrids (**1**-**2**) are detailed in this manuscript. Synthesized compounds were characterized applying nuclear magnetic resonance, Fourier-transform infra-red spectroscopy and single-crystal X-ray diffraction techniques. A detailed structural analysis of 3-(2-(5-(4-bromophenyl)-3-(4-fluorophenyl)-4,5-dihydropyrazol-1-yl)thiazol-4-yl)-2H-chromen-2-one (**1**) and 3-(2-(3,5-bis(4-bromophenyl)-4,5-dihydropyrazol-1-yl)thiazol-4-yl)-2H-chromen-2-one (**2**) is reported along with a detailed description of the noncovalent interactions and their evaluation using Hirshfeld surface analysis, emphasizing the structure-directing role of C—H···O, Br···π and π–π interactions. Finally, DFT energetics, molecular electrostatic potential (MEP), quantum theory of "atoms-in-molecules" (QTAIM) and non-covalent interaction plot (NCIplot) index computations have been used to further investigate the relative importance of two different π-stacking complexes observed in the solid state of both compounds, which are recurrent binding motifs in their crystal packing.

Introduction

On one hand, thiazole compounds have gained remarkable attention in the scientific community due to their several pharmacological and biological applications. For instance the thiazole ring has anti-inflammatory,[1] antiviral,[2] antibacterial,[3] antifungal,[4] antitubercular,[5] anti-HIV,[6] antitumoral[7] and anti-oxidant properties.[8] Furthermore, many commercial drugs exhibit thiazole ring as an active group.[9] In addition, it has been demonstrated that pyrazoline ring is a biologically relevant structural motif. Recently, several pyrazoline containing drugs such as phenylbutazone, mefobutazone, kebuzone[10] and ramifenazone[11] were found to have significant anti-inflammatory activity. Finally, it is well-known that pyrazoline derivatives present beneficial pharmaceutical effects like antifungal,[12] antitumor,[13] antibacterial,[14] and antidepressant[15] activities.

On the other hand, numerous antibiotics have coumarin moiety as a key structural core. For instance, coumarins have antibacterial activity against Gram-positive bacteria.[16–18] Two important drugs (dicoumarol and warfarin) contain coumarin ring and they are used as anticoagulant in veins, lungs and heart.[19] Coumarin also has other biological applications such as anti-HIV,[20] antihyperglycemic,[21] anticonvulsant,[22] antifungal,[23] antioxidant,[24] and antiproliferative.[25] Moreover, coumarin derivatives are used in dyes due to their excellent optical and photophysical properties.[26,27] Coumarin-thiazoles dyes are exploited as optical brighteners,[28,29] fluorescence labels,[30,31] non-linear optical materials,[32] solar energy absorbers, laser dyes and as two-photon absorption (TPA) materials.[33]

[a] M. Madni, Prof. S. Hameed
Department of Chemistry, Quaid-i-Azam University,
Islamabad 45320, Pakistan
E-mail: murtaza.madni@gmail.com
shameed@qau.edu.pk

[b] Dr. M. N. Ahmed, G. Abbasi
Department of Chemistry,
The University of Azad Jammu and Kashmir,
Muzaffarabad, 13100 Pakistan
E-mail: drnaeem@ajku.edu.pk

[c] Dr. M. A. A. Ibrahim
Computational Chemistry Laboratory,
Chemistry Department, Faculty of Science,
Minia University, Minia 61519, Egypt

[d] Prof. Muhammad N.Tahir, M. Ashfaq
Department of Physics, University of Sargodha,
Sargodha, Pakistan

[e] Prof. D. M. Gil
INBIOFAL (CONICET – UNT)
Instituto de Química Orgánica. Facultad de Bioquímica,
Química y Farmacia. Universidad Nacional de Tucumán.
Ayacucho 471. T4000INI. San Miguel de Tucumán,
Argentina Member of the research Career of CONICET

[f] Dr. R. M. Gomila, Prof. A. Frontera
Departament de Química, Universitat de les Illes Balears,
Crta. de Valldemossa km 7.5, 07122
Palma de Mallorca (Baleares), SPAIN
E-mail: toni.frontera@uib.es

ChemistrySelect

Research Article
doi.org/10.1002/slct.202202287

Chemistry Europe
European Chemical
Societies Publishing

Similar properties have been also described for substituted pyrazolyl thiazolyl coumarin dyes.[34–36]

In continuance of our previous work emphasizing the significance of antiparallel displaced π-stacking [37,38] and tetrel bonding[39,40] in crystal engineering,[41] in this manuscript we report the synthesis, spectroscopic and solid state characterization of two new pyrazolyl-thiazole-coumarin hybrids that present an extended π-surface due to the planarity of the pyrazolyl-thiazole-coumarin system that mostly dictate their X-ray packing (see Scheme 1). Several π-stacking modes and halogen bonding interactions have been also studied using DFT calculations and characterized by a combination of computational tools, such us molecular electrostatic potential (MEP) surfaces, the quantum theory of atoms-in-molecules and the noncovalent interaction plot (NCIPlot). Moreover, the relative importance of the interactions has been also analyzed by using Hirshfeld surface analysis.

Results and Discussion

Synthesis

The synthesis of compounds **1**–**2** were carried out using a slightly modified protocol (see Scheme 2).[26,42–45] That is, substituted chacones, thiosemicarbazide and sodium hydroxide were introduced in a two-neck round bottom flask and ethanol was used as solvent. The reaction mixture was stirred and refluxed to get 3,5-disubstituted phenyl-4,5-dihydropyrazole-1-carbothioamide. Subsequently, 3,5-disubstitutedphenyl-4,5-di-hydropyrazole-1-carbothioamide was added to a suspension of

3-(2-bromoacetyl)-2*H*-chromen-2-one in ethanol and stirred vigorously under reflux for 2 hours to obtain the target compounds (**1**–**2**).

### Description of crystal structures

The molecular structure of compounds **1** and **2** are shown in Figure 1. Compound **1** crystallizes in the triclinic crystal system with the centrosymmetric *P*-1 space group, while compound **2** crystallizes in the monoclinic system, space group *C*2/c. As shown in Figure 1b, compound **2** crystallizes with disordered CHCl₃ molecules.

In both compounds, the chromenone rings are nearly coplanar with the thiazole rings. The planar arrangement of both rings is mainly favored by intramolecular C17–H17···O2 hydrogen bonds [d(H···O) = 2.28 Å, < (C–H···O) = 118°] between the H17 atom of the thiazole ring and the O2 of the chromenone moiety as acceptor. In 1, the dihedral angle between the mean planes conformed by the bromophenyl (C1–C6) and thiazole rings is 5.58°. In 2, the bromophenyl ring is more twisted (6.27°) than in 1 with respect to the mean plane of the thiazole ring.

The C–S bond lengths of the thiazole ring in both compounds are in the range 1.712(4)–1.743(4) Å, and the C16–N3 bond lengths [1.296(6)–1.299(5)] are shorter than the C18–N3 [1.396(4)–1.401(5) Å] bond. The C7–N1 and N1–N2 bond lengths of the pyrazolyl ring are 1.293(5) and 1.374(5)–1.391(5) Å, respectively. These values, coupled with the observed planarity of these fragments are an indicative of some delocalization of π-electron density over these fragments.
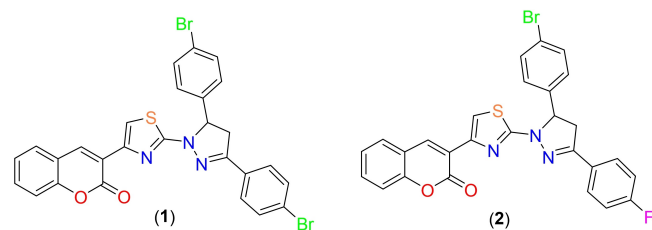
Scheme 1. Compounds **1**–**2** synthesized in this work.
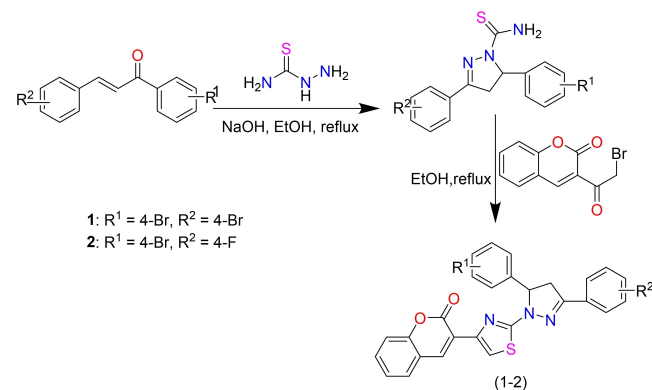
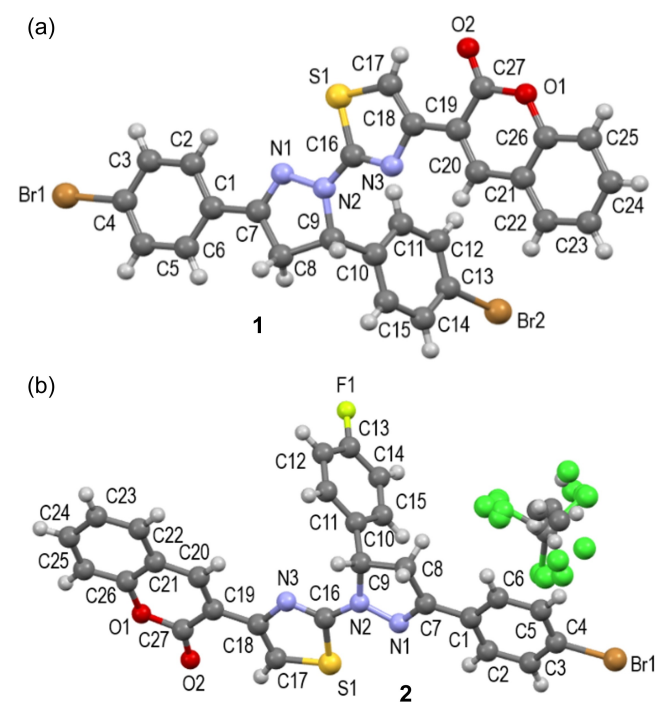**Scheme 2.** Synthetic route for the target compounds (**1**–**2**)

Figure 1. Molecular structure of compounds **1** (a) and **2** (b) determined by single crystal X-ray diffraction methods showing the labels of non-H atoms.

ChemistrySelect

Research Article
doi.org/10.1002/slct.202202287

Chemistry Europe
European Chemical
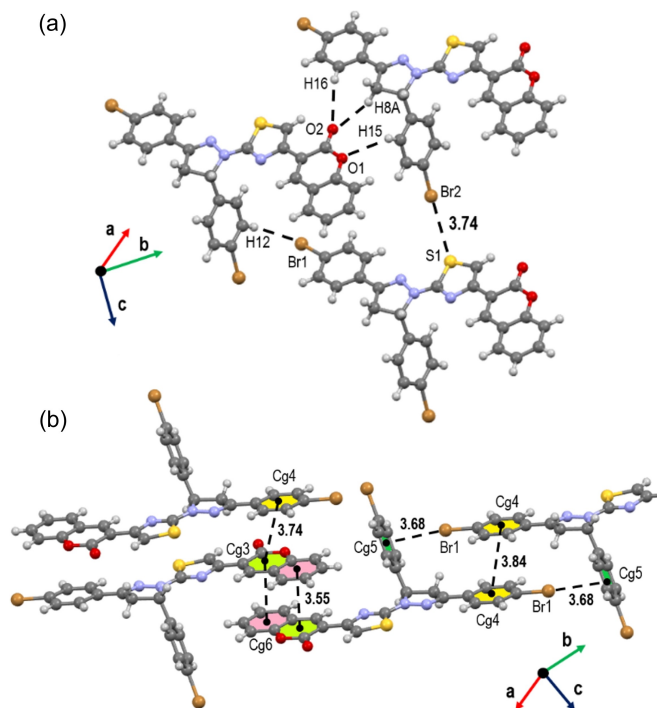Societies Publishing

(a)

(b)

Figure 2. (a, b) View of the crystal packing of compound **1**. The intermolecular contacts are shown as dashed lines. The definition of the centroids of the rings are discussed in the text. Distances in Å.

In the crystal packing, molecules of **1** are linked through C16–H16···O2, C8–H8 A···O2, C15-H15···O1 and C12–H12···Br1 hydrogen bonds (Figure 2a, Table 1). In addition to these hydrogen bonds, the molecular assembly is also stabilized by π···π stacking interactions between adjacent rings, with centroid to centroid distances between 3.5512(3) and 3.8398(4) Å (see Table 2, Figure 2b). Interestingly, there are Br···S halogen bonding interactions between the Br1 atom from the bromobenzene ring and the S1 atom of the thiazole moiety, as shown in Figure 2a [d(Br2···S1) = 3.736(3) Å, symmetry: x, y, z + 1]. The Br1 atoms of the bromobenzene moiety are orientated towards the π-face of the second bromobenzene ring (Cg5), as shown in Figure 2b. The distance between the bromide Br1 atom and the centroid Cg5 of the π-face is 3.6826(3) Å [α C4-Br1···Cg5 = 168.88(1)°], thus indicating significant halogen bond Br···π interactions.

Molecules of **2** are connected with each other through C8–H8B···O2, C9–H10···O2 and C17–H17···O2 hydrogen bonds (Figure 3a, Table 2). The H5 atom of the bromobenzene ring interacts with the F atom through C5–H5···F1 hydrogen bond [d(H5···F1) = 2.725(3) Å, ∠(C5-H5···F1) = 146.58(1)°]. The structure of **2** shows π···π stacking interactions with intercentroid Cg···Cg distances between 3.6863(4) and 3.8277(4) Å (see Table 2, Figure 3b). The crystal packing of **2** is also stabilized by intermolecular C–H···π interactions involving the fluorobenzene ring (Cg5) and the H22 [d(H22···Cg5) = 2.53 Å, ∠(C22–H22···Cg5) = 156°, symmetry: −x, y, ¹/₂−z] and H25 [d-

Table 1. Geometrical parameters of the hydrogen bonding interactions in compounds **1** and **2**.				
D–H···A Compound 1	d(D···A)	d(H···A)	<(D–H···A)	Symmetry
C15–H15···O1	3.366(3)	2.778(3)	122.08(1)	x, y−1, z
C6–H6···O2	3.685(3)	2.815(3)	154.14(1)	x, y−1, z
C8–H8B···O2	3.344(3)	2.466(3)	150.46(1)	x, y−1, z
Compound 2				
C5–H5···F1	3.539(3)	2.725(3)	146.58(1)	x, −y, z−1/2
C8–H8B···O2	3.308(3)	2.655(3)	124.96(1)	x, y−1, z
C9–H10···O2	3.508(3)	2.913(3)	120.07(1)	x, y−1, z
C17–H17···O2	3.270(3)	2.608(3)	128.6(1)	−x, −y+2, −z

Table 2. Geometrical parameters for the π-stacking interactions in compounds **1** and **2** (Å, °).							
Rings (I)-(J)[a] Compound **1**	Rc[b]	R1v[c]	R2v[d]	α[e]	β[f]	γ[g]	Symmetry
Cg3···Cg6	3.5512(3)	3.499	3.495	1.0	10.2	9.8	−x, 2−y, 1−z
Cg3···Cg4	3.7422(3)	3.504	3.489	5.0	21.2	20	−x, 1−y, −z
Cg4···Cg4	3.8398(4)	3.584	3.584	0.0	21.0	21	1−x, −y, −z
Compound **2**							
Cg4···Cg6	3.8277(4)	3.462	3.459	1.0	25.3	25	−x, 1−y, −z
Cg3···Cg3	3.6863(4)	3.651	3.651	14	7.90	7.9	−x, y, ¹/₂−z
Cg1···Cg2	3.7893(4)	3.486	3.611	5.0	17.6	23	−x, 1−y, −z
Cg3···Cg4	3.7036(4)	3.460	3.472	1.0	20.3	21	−x, 1−y, −z

[a]Cg1, Cg2, Cg3, Cg4 and Cg5 are the centroids of the rings S1/C16/N3/C18/C17, N1/N2/C9/C8/C7, O1/C25/C21/C20/C19/C27, C1-C6, C10-C15 and C21-C26, respectively. [b]Centroid distance between ring centroid I and J. [c]Vertical distance from ring centroid I to ring J. [d]Vertical distance from ring centroid J to ring I. [e]Dihedral angle between mean planes I and J. [f]Angle between the centroid vector Cg(I)···Cg(J) and the normal to the plane (I). [g]Angle between the centroid vector Cg(I)···Cg(J) and the normal to the plane (I).

ChemistrySelect

Research Article
doi.org/10.1002/slct.202202287

Chemistry
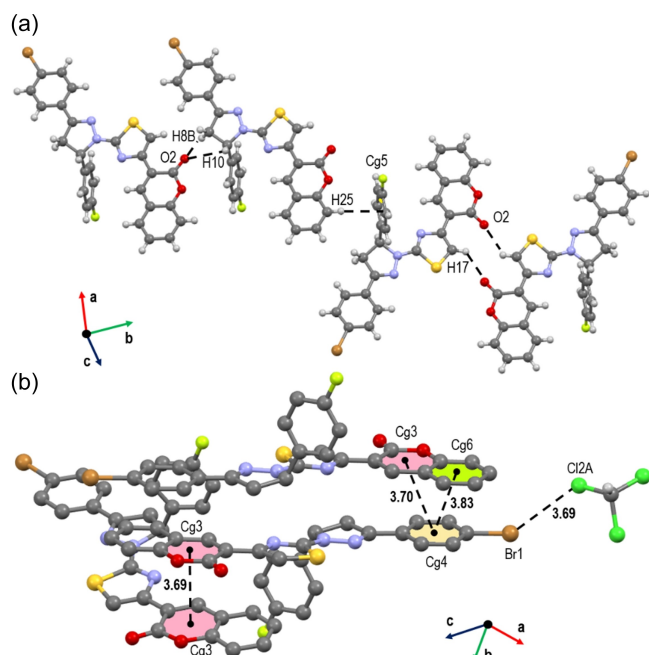**Europe**
European Chemical
Societies Publishing

Figure 3. (a, b) View of the crystal packing of compound **2**. The intermolecular contacts are shown as dashed lines. The definition of the centroids of the rings are discussed in the text. In (b) the H-atoms are omitted for clarity. Distances in Å.

(H25···Cg5) = 2.71 Å, ∠(C25–H25···Cg5) = 168°, symmetry: −x, 1 + y, ¹/₂−z] atoms. The crystal structure of **2** also shows Br···Cl halogen bonding interactions involving the bromide atom of the bromobenzene ring and the Cl2 A from the chloroform solvent molecule [d(Br1···Cl2 A) = 3.6965(3) Å, symmetry: x, −y, z-1/2].
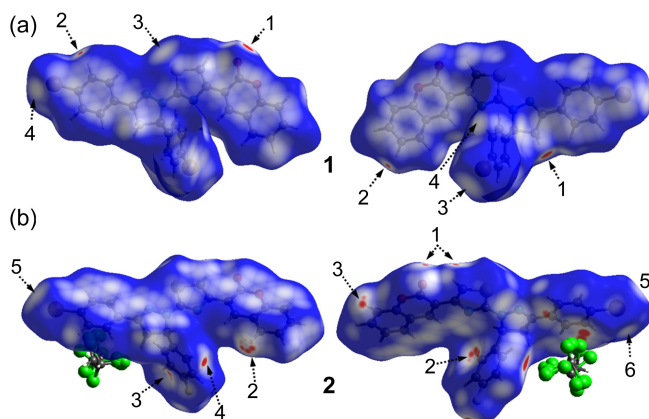

Figure 4. Hirshfeld surfaces of compounds **1** and **2** mapped with d_{norm} function in two orientations. The second molecule is 180° rotated around the horizontal axis of the plot. The labels are discussed in the main text.

Hirshfeld surface analysis

The Hirshfeld surfaces of **1** and **2** are shown in Figure 4, illustrating surfaces that have been mapped over d_{norm} property. The dominant interactions in both compounds can be seen as the bright red areas. Full 2D-fingerprint plots of the main intermolecular interactions are depicted in Figure 5.

In compound **1**, the red spots labeled 1 in the HSs are attributed to intermolecular C8-H8 A···O2 hydrogen bonds involving the H8 A atom of the dihydropyrazolyl moiety and the O2 atom as acceptor. These interactions are also visible in the FP plots as a pair of symmetrical spikes at $(d_e + d_i) \cong 2.35$ Å with a contribution of 9.10% to the total Hirshfeld surface area. The presence of H···H contacts in the crystal packing of **1** is evidenced by the visible bright red areas labeled 2 in the d_{norm} surface attributed to H3···H23 dihydrogen interactions [d-(H···H) = 2.359 Å], with a distance shorter than the sum of vdW radii of H-atoms. These H···H contacts are highlighted in the middle of the scattered points of the FP map (labeled 1) with a minimum value of $(de + di) \cong 2.10$ Å and the highest contribution of 31.5% to the total Hirshfeld surface.

As can be seen in Figure 4, the crystal packing of **1** is stabilized by Br2···S1 halogen bonding interactions. The distance Br···S in this compound [d(Br2···S1) = 3.736 Å] is slightly shorter than the sum of the vdW radii (3.75 Å).[46] These contacts are visible in the d_{norm} map as white spots labeled 3. In addition, the HSs of **1** show two white areas labeled 4 associated to C12–H12···Br1 hydrogen bonds. These interactions are visible in the FP plots as sharp spikes (labeled 3 in Figure 2a) at around $(d_e + d_i) \cong 2.90$ Å, in accordance with the H12···Br1 of 3.065 Å. These H···Br/Br···H contacts comprise 18.6% of the total HS area. As shown in Figure 2a, the broad spikes observed in the full FP plot of **1** is mainly attributed to H···C/C···H contacts with a large area fraction of 13.6%.

In compound **2**, the red regions located around the H17 and O2 atoms are attributed to C17–H17···O2 hydrogen bonds, with 8.9% contribution to the HS area. Similarly to compound **1**, the crystal structure of **2** is also stabilized by H11···H11 dihydrogen interactions. These contacts are visible in the d_{norm} surface as red spots labeled 4 and comprise 21.2% of the total HS area. The small red spots labeled 2 and 3 in the d_{norm} surface
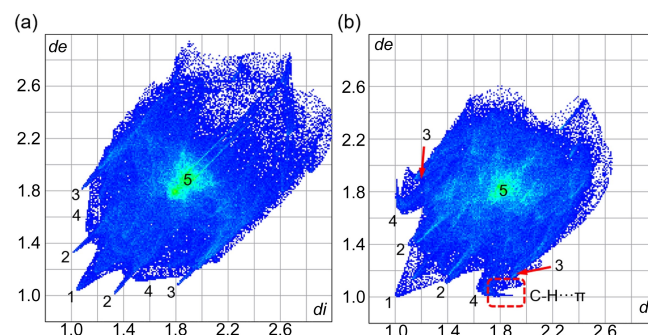

Figure 5. Full two-dimensional fingerprint plots for compounds **1** (a) and **2**. (b) Close contacts are labelled as follows: (1) H···H, (2) H···O/O···H, (3) H···Br/Br···H, (4) H···C/C···H, (5) C···C.

ChemistrySelect

Research Article
doi.org/10.1002/slct.202202287

**Chemistry
Europe**
European Chemical
Societies Publishing

of **2** are attributed to C—H···π interactions, involving the H22 and H25 atoms and the centroid Cg5 of the C10–C15 ring, respectively. These C—H···π contacts are visible as a pair of wings in the top left and bottom right region in the FP plots (see Figure 2b), which comprise 16.3% of the total Hirshfeld surface area. The white spots labeled 5 in the HSs of **2** are mainly attributed to Br1···Cl2 A halogen bonding interactions involving the Br1 atoms of the bomobenzene ring and the chlorine atom of the chloroform solvent molecule. The white spot labeled 6 in the d_{norm} map is associated to C14–H14···Br1 hydrogen bonds [d(H14···Br1) = 3.191 Å]. These H···Br/Br···H contacts are evident in the FP plots (Figure 2b) as broad spikes at $(d_e + d_i) \cong 3.10$ Å and comprise 7.5% of the total Hirshfeld surface area.

We have mapped the Hirshfeld surfaces with shape index and curvedness properties to identify planar π-π stacking interactions, which generally are not clearly visible in the analysis of the crystal structures.[47] The shape index surfaces of both compounds (Figure 6, column 1) show a pattern of touching red and blue triangles highlighted with dashed circles, thus indicating the existence of π-π stacking interactions (see Table 2). These contacts are also visible as relatively large and green plat regions delineated by blue circles on the curvedness surfaces of both compounds (Figure 6, column 2). Finally, the C···C contacts involved in the π-π stacking interactions appear as a distinct pale blue to green area labeled 5 in the FP plots of both compounds at around $d_e = d_i = 1.8$ Å, with major contributions of 10.1% and 8.8% for compounds **1** and **2**, respectively.

DFT study

First, we have computed the molecular electrostatic potential (MEP) surfaces of compounds **1** and **2** to investigate the most electrophilic and nucleophilic parts of the molecules. Moreover, we are also interested in the existence and magnitude of σ-holes on the extensions of the C—Br bonds

Figure 7 shows the MEP surfaces of compounds **1** and **2** evidencing the existence of the σ-holes at the Br-atoms that range from +10.9 to +12.2 kcal/mol (see Table 3). The MEP
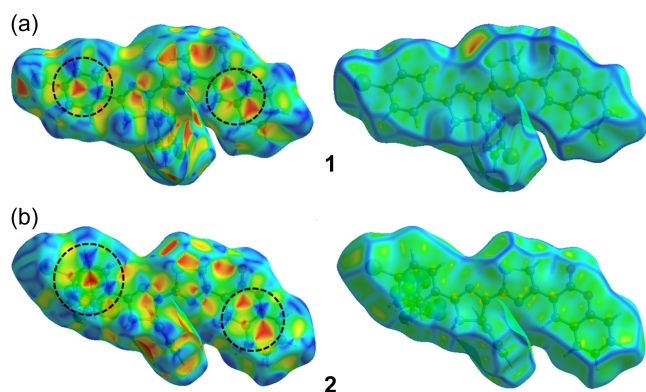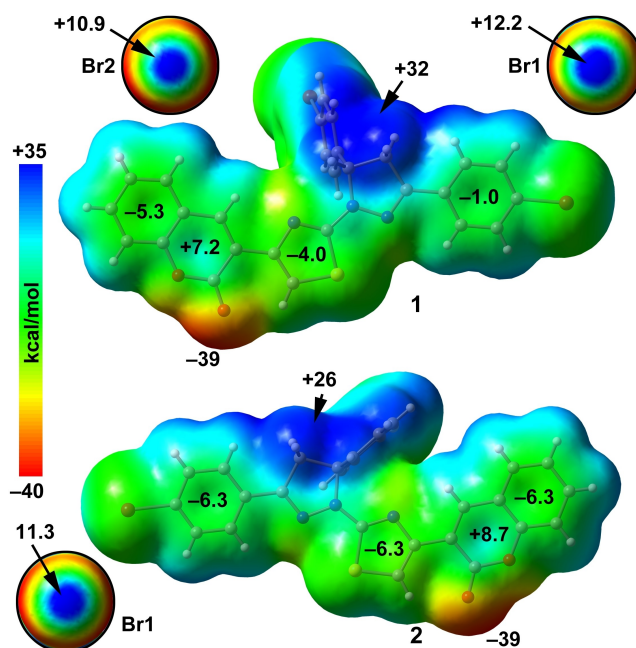

Figure 7. MEP surfaces (isosurface 0.001 a.u.) of compounds **1** (a) and **2** (b). Detail of the MEP surface around the Br-atoms are given next to the corresponding Br atoms of the global surface, using a more reduced scale (± 12 kcal/mol). The energies are given in kcal/mol.

Table 3. MEP values (kcal/mol) at selected points of the surfaces for compounds **1**–**2** at the PBE0-D3/def2-TZVP level of theory.

Compound	$V_{s,max}$	$V_{s,min}$	$V_{s,Br1}$	$V_{s,Br2}$	$V_{s,\pi}$ [a]
1	+32	−39	+12.2	+10.9	−5.3/+7.2
2	+26	−39	+11.3	–	−6.3/+8.7

[a]MEP values over the phenyl and pyranone rings (positive and negative, respectively) of the chromenone system are gathered.

Figure 6. Hirshfeld surfaces of compounds **1** and **2** mapped over shape index (left) and curvedness (right) properties.

surfaces also show that the MEP maxima are located at the aliphatic C—H bonds of dihydropyrazole ring in both complexes. The MEP minimum is located at the O-atom of the carbonyl group in both compounds with identical value (−39 kcal/mol). This analysis and the location of the MEP maximum and minimum agrees well with the important C—H··O interactions described above in both compounds, which are relevant in their crystal packing.

It is worthy to highlight the π-acidic/basic dualism of the chromenone system. Specifically, the MEP value is positive over the center of the 4-pyranone ring and negative over the center of the phenyl ring. Thus, the formation of the antiparallel π-stacked in compound **1** (see Figure 2b) can be rationalized by this anisotropy of the electron density in the chromenone system. The MEP values over the thiazole and bromophenyl rings are also negative.

For compound **1**, we have analysed two different antiparallel π-stacking modes observed in the solid state by using a combination of QTAIM and NCIplot index computational tools. The plots are represented in Figure 8 showing only intermolecular interactions for the sake of clarity. In the first one, the π-
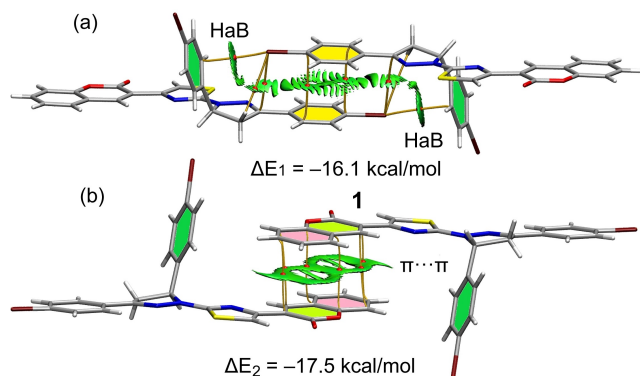
ChemistrySelect

Research Article
doi.org/10.1002/slct.202202287

Chemistry Europe
European Chemical
Societies Publishing

Figure 8. (a,b) Combined QTAIM/NCIplot analyses of two self-assembled π-stacked dimers of compound **1**. Only bond critical points are represented (as red spheres), for the sake of clarity. For the NCIplot isosurface ($s=0.5$), the $-0.35 < \mathrm{sign}(\lambda_2)\rho < 0.35$ colour scale was used. Gradient cut-off $=0.04$ a.u.

stacking is established between the bromophenyl rings in combination with two symmetrically equivalent halogen bonds (HaB). The HaB is characterized by a bond critical point (CP) and bond path connecting the Br and one C-atom of the aromatic ring, thus confirming the formation of the HaBs. The π···π stacking is characterized by two bond CPs and bond paths interconnecting the rings. Both interactions are also characterized by RDG green isosurfaces, confirming their attractive nature. The QTAIM analysis also shows some additional contacts between the negative belt of the Br-atom and the electrophilic dihydropyrazole ring. Such combination of interactions explains the large binding energy observed for this π-stacking mode ($\Delta E_1 = -16.1$ kcal/mol). Figure 8b shows the other π-stacking mode that only involves the chromenone moieties, which are antiparallel oriented. Four bond CPs and bond paths interconnect the chromenone rings. The NCIplot shows an extended green isosurface that embraces the whole space between both chromenone moieties, confirming the strong complementarity of the antiparallel π-stacking. Such orientation agrees well with the π-acidic/basic duality commented above and explains the large interaction energy ($\Delta E_2 = -17.5$ kcal/mol).

Additional analysis of the Br···S halogen bond (see Figure 2a) described above for compound **1** is included in the ESI (see Figure S1). Regarding compound **2**, the π-stacked self-assemblies observed in compound **1** are not observed, likely due the presence of the solvent molecules that interact with several rings, as described in the ESI (Figure S2). A common feature of both compounds is the formation of self-assembled dimers where the bromobenzene, chromenone and 4,5-dihydropyrazolylthiazole moieties participate, as detailed in Figure 9. This intricate combination of interactions includes two symmetrically equivalent π-stacking interactions between the chromenone and the bromobenzene rings, an antiparallel displaced π-stacking between the 4,5-dihydropyrazolylthiazole moieties and CH···O contacts between the CH groups of the 4,5-dihydropyrazole rings and the O-atoms of the carbonyl groups. The formation of latter interactions reinforcing the
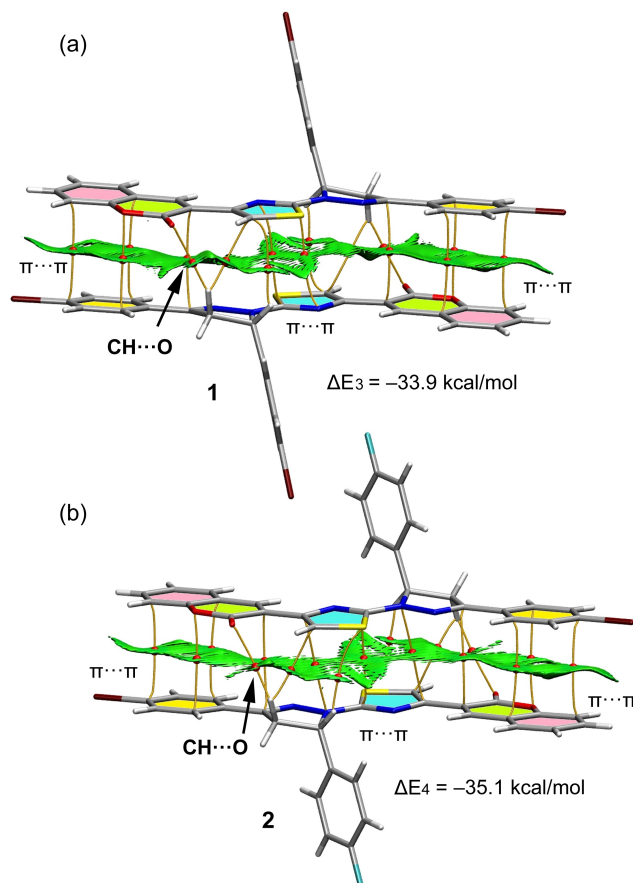

Figure 9. Combined QTAIM/NCIplot analyses of two self-assembled π-stacked dimers of compound **1** (a) and **2** (b). Only bond CPs are shown (as red spheres), for clarity. For the NCIplot isosurface ($s=0.5$), the $-0.35 < \mathrm{sign}(\lambda_2)\rho < 0.35$ colour scale was used. Gradient cut-off $=0.04$ a.u.

dimer is in line with the MEP surface analysis (see Figure 7), showing large MEP values in both groups. This myriad of interactions is confirmed by multitude bond CPs, bond paths connecting both monomers and a large NCIplot isosurface that embraces the whole interface between both molecules, disclosing the strong complementarity of both molecules upon formation of the π-stacked dimers. As a consequence, the dimerization energies are very large, that is $\Delta E_3 = -33.9$ kcal/mol and $\Delta E_4 = -35.1$ kcal/mol for **1** and **2**, respectively, validating the relevance role of such dimers in the crystal packing of both compounds

Conclusion

Two new 4,5-dihydropyrazolylthiazole-coumarin hybrids were synthesized and X-ray characterized. Their ability to self-assemble via π-stacking in the solid-state were studied using HS analysis, theoretical calculations, and a combination of QTAIM and NCIPlot methods. These studies disclosed that antiparallel π···π stacking interactions are the most dominant interactions, having a crucial role in the solid-state architecture of both complexes. We hope that the results reported herein

ChemistrySelect

Research Article
doi.org/10.1002/slct.202202287

Chemistry Europe
European Chemical
Societies Publishing

are useful for researchers working on crystal engineering and supramolecular chemistry when screening an appropriate combination of aromatic/non-aromatic rings in the design of novel organic molecules with π-extended systems.

Experimental Section

The synthesis of compounds **1–2** was carried out by following a procedure reported in literature.[26,42] The compounds were characterized by IR, NMR and single crystal X-ray crystallography. Yanaco melting point apparatus was used to determine the melting points, which are given uncorrected. Thermoscientific Fourier Transform Infra-Red Spectrophotometer USA model nicolet 6700 using Attenuated total reflectance (ATR) facility was used to record the FT-IR spectra of **1** and **2**. A Bruker Avance 300 MHz spectrophotometer in CDCl$_3$ solution was used to acquire the NMR spectra. Chemical shifts (δ) are reported in ppm downfield from TMS. Chemical shifts were calibrated relative to residual solvent signal.

3-(2-(3,5-Bis(4-bromophenyl)-4,5-dihydropyrazol-1-yl)thiazol-4-yl)-2H-chromen-2-one (1)

Colour pale yellow solid, Yield: 83%, Mp 220–222°C; Rf: 0.47 (*n*-hexane:ethyl acetate; 7:3); FTIR (ν$_{max}$, cm^{-1}): 1703 (C=O), 2976 (C–H), 3039 (C=C–H); ^{1}HNMR (300 MHz, DMSO-d$_6$): δ = 3.29 (dd, 1H, J$_{cis}$ = 7.5 Hz, J$_{gem}$ = 17.4 Hz, CH-pyrazoline), 3.92 (dd, 1H, J$_{trans}$ = 12.0 Hz, J$_{gem}$ = 17.4 Hz, CH-pyrazoline), 5.62 (dd, 1H, J$_{cis}$ = 7.5 Hz, J$_{trans}$ = 12.0 Hz, CH-pyrazoline), 7.31–7.86 (m, 13H, Ar), 8.15 (s, 1H, CH-thiazole); ^{13}CNMR (75 MHz, DMSO-d$_6$): δ = 43.33, 64.61, 111.97, 116.30, 119.34, 119.64, 121.92, 124.31, 124.44, 127.80, 128.15, 128.33, 130.07, 131.10, 131.93, 132.00, 138.41, 138.60, 140.55, 151.77, 152.81, 160.11, 165.00.

3-(2-(5-(4-bromophenyl)-3-(4-fluorophenyl)-4,5-dihydropyrazol-1-yl)thiazol-4-yl)-2H-chromen-2-one (2)

Pale yellow solid, **Yield**: 85%, Mp 240–242°C; Rf: 0.41 (*n*-hexane: ethyl acetate; 7:3); FTIR (ν$_{max}$, cm^{-1}): 1711 (C=O), 2969 (C–H), 3042 (C=C–H). ^{1}HNMR (300 MHz, DMSO-d$_6$): δ = 3.45 (dd, 1H, J$_{cis}$ = 7.2 Hz, J$_{gem}$ = 18.0 Hz, CH-pyrazoline), 4.08 (dd, 1H, J$_{trans}$ = 11.7 Hz, J$_{gem}$ = 18.0 Hz, CH-pyrazoline), 5.71 (dd, 1H, J$_{cis}$ = 7.2 Hz, J$_{trans}$ = 11.7 Hz, CH-pyrazoline), 7.25–7.80 (m, 13H, Ar), 8.25 (s, 1H, CH-thiazole), ^{13}CNMR (75 MHz, DMSO-d$_6$): δ = 43.25, 64.49, 111.79, 115.64, 116.38, 119.53, 120.89, 123.85, 125.26, 128.84, 129.12, 129.81, 129.92, 130.58, 132.19, 132.30, 138.11, 138.79, 144.29, 152.77, 152.92, 159.06, 163.70.

Crystal data and structure refinement

A Bruker Kappa APEXII CCD X-ray diffractometer having graphite monochromated Mo–Kα radiation (λ = 0.71073 Å) was used for the single crystal x-ray diffraction of compounds (**1–2**). The needle and rod shaped single crystals of **1** and **2**, respectively appropriate for X-ray investigation were acquired from EtOH/EtOAc and placed on a glass fiber in order to collect data on Bruker Apex-II software.[48] Direct methods and difference fourier maps on SHELXS97[49] were used to solve the structures effectively. Subsequentlly, they were refined on the square of atomic factors by a full-matrix least-squares procedure and using anisotropic displacement parameters. H-atoms in compounds **1** and **2** were sited in ideal positions. They were refined as riding atoms with relative isotropic displacement

parameters. SHELXL-2018/3 and WinGX-2014.1 programs[50,51] were used for all refinements The method to collect data was ω-scans and data integration. They were performed using the Bruker SAINT[52] software package. The crystallographic illustrations for the structures were prepared by utilizing ORTEP-3.[51] Experimental parameters related to single-crystal X-ray inspection of compounds are given in Table 4.

Hirshfeld surface calculations

The Hirshfeld surfaces (HSs) and their associated two-dimensional fingerprint plots (FP)[53–56] were generated using the CrystalExplorer21 software.[57] The 3D HSs were mapped over d_{norm} (normalized contact distance), shape index and curvedness. Each point on the surface provides information regarding the distance between specific point on the surface to the closest interior atom (d_i), surface point to nearest exterior atom distance (d_e) and van der Waals (vdW) radii of atoms. The distances equal to the sum of vdW atomic radii are represented as white regions and the contacts with distances shorter and longer than the sum of vdW atomic radii are shown as red and blue colours, respectively. The d_{norm} surfaces were mapped over a fixed colour scale of −0.05 a.u. (red) to 0.58 a.u. (blue). We have analysed two additional coloured properties namely shape index and curvedness based on the local curvature of the surface. The 2D FP plots give exclusive information about contribution of each interior to exterior atomic non-covalent interactions through the Hirshfeld surface. The FP plots were generated by using the translated (1.0–2.8 Å) range, and reciprocal contacts were included.

Table 4. X-ray details of compounds 1–2.		
Compound #	1	2
CCDC	2143901	2143902
Chemical formula	C$_{27}$H$_{17}$Br$_2$N$_3$O$_2$S	C$_{28}$H$_{18}$BrCl$_3$FN$_3$O$_2$S
M_r	607.32	665.77
Space group	P-1	C2/c
Temperature (K)	296	296
a (Å)	9.7375 (9)	34.113 (3)
b (Å)	11.620 (1)	9.7519 (10)
c (Å)	12.051 (1)	19.3756 (19)
α (°)	114.207 (4)	90
β (°)	97.345 (5)	119.579 (4)
γ (°)	90.391 (4)	90
V (Å^3)	1230.82 (19)	5605.5 (10)
Z	2	8
Radiation type	Mo Kα	Mo Kα
μ (mm^{-1})	3.41	1.87
Crystal size (mm)	0.40×0.20×0.16	0.38×0.26×0.24
T_{min}, T_{max}	0.440, 0.646	0.510, 0.610
No. of measured, independent and observed [$I > 2σ(I)$] reflections	19049, 5372, 2806	20548, 5484, 2854
R_{int}	0.053	0.046
(sin θ/λ)$_{max}$ (Å^{-1})	0.640	0.617
$R[F^2 > 2σ(F^2)]$, $wR(F^2)$, S	0.049, 0.110, 1.00	0.051, 0.131, 1.00
No. of reflections	5372	5484
No. of parameters	316	465
No. of restraints	–	528
Δ&yτ";$_{max}$, Δ&yτ";$_{min}$ (e Å^{-3})	0.70, −0.69	0.42, −0.52

ChemistrySelect

Research Article
doi.org/10.1002/slct.202202287

**Chemistry
Europe**
European Chemical
Societies Publishing

Theoretical methods

The energies and topological analyses of the supramolecular assemblies investigated herein were computed at the RI-BP86-D3/def2-TZVP level of theory[58,59] using the crystallographic coordinates and the program Turbomole 7.2.[60] Grimme's D3 dispersion[61] correction has been used since it is convenient for the correct evaluation of noncovalent interactions and specially those involving π-systems. The quantum theory of atoms in molecules (QTAIM)[62] and noncovalent interaction (NCI) plot[63] reduced density gradient (RGD) isosurfaces have been used to characterize non-covalent interactions. Both methods combined are useful to reveal noncovalent interactions in real space. The wavefunctions needed to generate the NCIplot surfaces have been computed at the same level of theory using the Turbomole 7.2 program. The NCIPlot index RDG isosurfaces correspond to both favourable and unfavourable interactions, as differentiated by the sign of the second density Hessian eigenvalue and defined by the isosurface colour. The colour code used in this manuscript is blue and green for attractive interactions (strong and weak, respectively) and yellow and red for weakly and strongly repulsive, respectively. The NCIPlot cubes needed to construct the isosurfaces have been computed by means of the MULTIWFN program[63] and represented using VMD software.[64]

Conflict of Interest

The authors declare no conflict of interest.

Data Availability Statement

The data that support the findings of this study are available in the supplementary material of this article.

[1] Z. A. Muhammad, G. S. Masaret, M. M. Amin, M. A. Abdallah, T. A. Farghaly, *Med. Chem.* **2017**, *13*, 226–238.

[2] I. P. Singh, S. Gupta, S. Kumar, *Med. Chem.* **2020**, *16*, 4–23.

[3] K. Z. Laczkowski, A. Biernasiuk, A. Baranowska-Laczkowska, K. Misiura, A. Malm, T. Plech, A. Paneth, *Med. Chem.* **2016**, *12*, 553–562.

[4] C. I. Lino, I. G. De Souza, B. M. Borelli, T. T. S. Matos, I. N. S. Teixeira, J. P. Ramos, E. M. De Souza Fagundes, P. De Oliveira Fernandes, V. G. Maltarollo, S. Johann, *Eur. J. Med. Chem.* **2018**, *151*, 248–260.

[5] Y. K. Abhale, A. Shinde, K. K. Deshmukh, L. Nawale, D. Sarkar, P. C. Mhaske, *Med. Chem. Res.* **2017**, *26*, 2557–2567.

[6] M. Madni, S. Hameed, M. N. Ahmed, M. N. Tahir, N. A. Al-Masoudi, C. Pannecouque, *Med. Chem. Res.* **2017**, *26*, 2653–2665.

[7] Y. Lu, C.-M. Li, Z. Wang, C. R. Ross, J. Chen, J. T. Dalton, W. Li, D. D. Miller, *J. Med. Chem.* **2009**, *52*, 1701–1711.

[8] O. S. Afifi, O. G. Shaaban, H. A. A. El Razik, S. E.-D. A. S. El, F. A. Ashour, A. A. El-Tombary, M. M. Abu-Serie, *Bioorg. Chem.* **2019**, *87*, 821–837.

[9] O. I. El-Sabbagh, M. M. Baraka, S. M. Ibrahim, C. Pannecouque, G. Andrei, R. Snoeck, J. Balzarini, A. A. Rashad, *Eur. J. Med. Chem.* **2009**, *44*, 3746–3753.

[10] F. Jorquera, M. Almar, A. Jimeno, M. Gonzalez-Sastre, J. Gonzalez-Gallego, *J. Pharma. Biomed. Anal.* **1995**, *13*, 1141–1145.

[11] A. K. Tewari, P. Srivastava, V. P. Singh, A. Singh, R. K. Goel, C. G. Mohan, *Chem. Pharm. Bull.* **2010**, *58*, 634–638.

[12] P. S. Mahajan, M. D. Nikam, A. V. Chate, A. S. Bobade, C. H. Gill, *J. Heterocycl. Chem.* **2017**, *54*, 44–50.

[13] M. M. Edrees, S. A. Melha, A. M. Saad, N. A. Kheder, S. M. Gomha, Z. A. Muhammad, *Molecules* **2018**, *23*, 2970.

[14] Shubhalaxmi, L. Pathak, K. Ananda, K. S. Bhat, *Cogent Chem.* **2016**, *2*, 1141388.

[15] Y. R. Prasad, A. L. Rao, L. Prasoona, K. Murali, P. R. Kumar, *Bioorg. Med. Chem. Lett.* **2005**, *15*, 5030–5034.

[16] A. Kamal, K. S. Reddy, M. N. A. Khan, R. V. Shetti, M. J. Ramaiah, S. Pushpavalli, C. Srinivas, M. Pal-Bhadra, M. Chourasia, G. N. Sastry, *Bio. Med. Chem.* **2010**, *18*, 4747–4761.

[17] F. Azam, B. A. El-gnidi, I. A. Alkskas, M. A. Ahmed, *J. Enzyme Inhib. Med. Chem.* **2010**, *25*, 818–826.

[18] R. N. Sharma, F. P. Xavier, K. K. Vasu, S. C. Chaturvedi, S. S. Pancholi, *J. Enzyme Inhib. Med. Chem.* **2009**, *24*, 890–897.

[19] I. Kostova, S. Raleva, P. Genova, R. Argirova, *Bioinorg. Chem. Appl.* **2006**, *2006*, 1–9.

[20] C. Spino, M. Dodier, S. Sotheeswaran, *Bioorg. Med. Chem. Lett.* **1998**, *8*, 3475–3478.

[21] R. Kenchappa, Y. D. Bodke, A. Chandrashekar, M. A. Sindhe, S. Peethambar, *Arab. J. Chem.* **2017**, *10*, S3895-S3906.

[22] M. Mohammadi-Khanaposhtani, N. Ahangar, S. Sobhani, P. H. Masihi, A. Shakiba, M. Saeedi, T. Akbarzadeh, *Bioorg. Chem.* **2019**, *89*, 102989.

[23] S. Sardari, Y. Mori, K. Horita, R. G. Micetich, S. Nishibe, M. Daneshtalab, *Bioorg. Med. Chem.* **1999**, *7*, 1933–1940.

[24] J. Yu, L. Wang, R. L. Walzem, E. G. Miller, L. M. Pike, B. S. Patil, *J. Agricult. Food Chem.* **2005**, *53*, 2009–2014.

[25] A. Thakur, R. Singla, V. Jaitak, *Eur. J. Med. Chem.* **2015**, *101*, 476–495.

[26] M. Madni, M. N. Ahmed, S. Hameed, S. W. A. Shah, U. Rashid, K. Ayub, M. N. Tahir, T. Mahmood, *J. Mol. Struct.* **2018**, *1168*, 175–186.

[27] S. Ben Mohamed, Y. Rachedi, M. Hamdi, F. Le Bideau, C. Dejean, F. Dumas, *Eur. J. Org. Chem.* **2016**, *2016*, 2628–2636.

[28] A. Al-Kawkabani, M. Makhloufi-Chebli, N. Benosmane, B. Boutemeur-Kheddis, M. Hamdi, A. M. Silva, *J. Mol. Struct.* **2017**, *1146*, 285–291.

[29] H. N. Harishkumar, K. M. Mahadevan, J. N. Masagalli, *South African J. Chem.* **2012**, *65*, 5–9.

[30] K. Vaarla, R. K. Kesharwani, K. Santosh, R. R. Vedula, S. Kotamraju, M. K. Toopurani, *Bioorg. Med. Chem. Lett.* **2015**, *25*, 5797–5803.

[31] X. Yu, D. Scheller, O. Rademacher, T. Wolff, *J. Org. Chem.* **2003**, *68*, 7386–7399.

[32] S. H. Mashraqui, H. Mistry, S. Sundaram, *J. Heterocycl. Chem.* **2006**, *43*, 917–923.

[33] X. Li, Y. Zhao, T. Wang, M. Shi, F. Wu, *Dyes Pigm.* **2007**, *74*, 108–112.

[34] K.-L. An, K. H. Park, K. Jun, *Bull. Korean Chem. Soc.* **2014**, *35*, 2183–2185.

[35] H. G. Bonacorso, M. B. Rodrigues, W. C. Rosa, L. B. Silva, C. P. Frizzo, N. Zanatta, M. A. Martins, *J. Fluorine Chem.* **2015**, *178*, 296–305.

[36] D. P. Specht, P. A. Martic, S. Farid, *Tetrahedron* **1982**, *38*, 1203–1211.

[37] M. N. Ahmed, M. Arif, F. Jabeen, H. A. Khan, K. A. Yasin, M. N. Tahir, A. Franconetti, A. Frontera, *New J. Chem.* **2019**, *43*, 8122–8131.

[38] M. N. Ahmed, S. Shabbir, B. Batool, T. Mahmood, U. Rashid, K. A. Yasin, M. N. Tahir, M. A. Cassará, D. M. Gil, *J. Mol. Struct.* **2021**, *1236*, 130283.

[39] M. N. Ahmed, K. Y. Ansar, S. Aziz, S. Khan, M. N. Tahir, D. M. Gil, A. Frontera, *CrystEngComm* **2020**, *22*, 3567–3578.

[40] M. N. Ahmed, M. Ghias, S. W. A. Shah, M. Shoaib, M. N. Tahir, M. Ashfaq, M. A. Ibrahim, H. Andleeb, D. M. Gil, A. Frontera, *New J. Chem.* **2021**, *45*, 19928–19940.

[41] M. N. Ahmed, M. Madni, S. Anjum, S. Andleeb, S. Hameed, A. M. Khan, M. Ashfaq, M. N. Tahir, D. M. Gil, A. Frontera, *CrystEngComm* **2021**, *23*, 3276–3287.

[42] M. Madni, S. Hameed, M. N. Ahmed, K. A. Yasin, M. N. Tahir, *Chinese J. Struct. Chem.* **2015**, *7*, 1013–1018.

[43] Y.-M. Lin, Y. Zhou, M. T. Flavin, L.-M. Zhou, W. Nie, F.-C. Chen, *Bioorg. Med. Chem.* **2002**, *10*, 2795–2802.

ChemistrySelect

Research Article
doi.org/10.1002/slct.202202287

Chemistry Europe
European Chemical
Societies Publishing

[44] B. F. Abdel-Wahab, H. A. Abdel-Aziz, E. M. Ahmed, *Eur. J. Med. Chem.* **2009**, *44*, 2632–2635.

[45] M. Madni, M. N. Ahmed, M. Hafeez, M. Ashfaq, M. N. Tahir, D. M. Gil, B. Galmés, S. Hameed, A. Frontera, *New J. Chem.* **2020**, *44*, 14592–14603.

[46] S. Alvarez, *Dalton Trans.* **2013**, *42*, 8617–8636.

[47] a) S. K. Seth, *Acta Crystallogr.* **2018**, *E74*, 600–606; b) A. Di Santo, H. Pérez, G. A. Echeverría, O. E. Piro, R. A. Iglesias, R. E. Carbonio, A. Ben Altabef, D. M. Gil, *RSC Adv.* **2018**, *8*, 23891–23902; c) M. Rocha, M. C. Ruiz, G. A. Echeverría, O. E. Piro, A. L. Di Virgilio, I. E. León, A. Frontera, D. M. Gil, *New J. Chem.* **2019**, *43*, 18832–18842.

[48] A. Bruker, *Bruker AXS Inc.*, Madison, Wisconsin, USA, **2009**.

[49] G. M. Sheldrick, *Acta Crystallogr.* **2008**, *A64*, 112–122.

[50] G. M. Sheldrick, *Acta Crystallogr.* **2015**, *C71*, 3–8.

[51] L. J. Farrugia, *J. Appl. Crystallogr.* **2012**, *45*, 849–854.

[52] S. Bruker, Inc., Madison, Wisconsin, USA, **2013**.

[53] M. A. Spackman, P. G. Byrom, *Chem. Phys. Lett.* **1997**, *267*, 215–220.

[54] J. J. McKinnon, M. A. Spackman, A. S. Mitcel, *Acta Crystallogr.* **2007**, *B60*, 627–668.

[55] M. A. Spackman, D. Jayatilaka, *CrystEngComm.* **2009**, *11*, 19–32.

[56] J. J. McKinnon, D. Jayatilaka, M. A. Spackman, *Chem. Commun.* **2007**, 37, 3814–3816.

[57] P. R. Spackman, M. J. Turner, J. J. McKinnon, S. K. Wolff, D. J. Grimwood, D. Jayatilaka, M. A. Spackman, *J. Appl. Crystallogr.* **2021**, *54*, 1006–1011.

[58] S. Grimme, J. Antony, S. Ehrlich, H. Krieg, *J. Chem. Phys.* **2010**, *132*, 154104.

[59] F. Weigend, *Phys. Chem. Chem. Phys.* **2006**, *8*, 1057.

[60] R. Ahlrichs, M. Bär, M. Hacer, H. Horn, C. Kömel, *Chem. Phys. Lett.* **1989**, *162*, 165.

[61] R. F. W. Bader, *Chem. Rev.* **1991**, *91*, 893–928.

[62] J. Contreras-Garcia, E. R. Johnson, S. Keinan, R. Chaudret, J. P. Piquemal, D. N. Beratan, W. Yang, *J. Chem. Theory Comput.* **2011**, *7*, 625.

[63] T. Lu, F. Chen, *J. Comput. Chem.* **2012**, *33*, 580–592.

[64] J. W. Humphrey, A. Dalke, K. Schulten, *J. Mol. Graphics* **1996**, *14*, 33–38.